Magnetic resonance microimaging of intraaxonal water diffusion in live excised lamprey spinal cord

Masaya Takahashi*†, David B. Hackney*, Guixin Zhang‡, Suzanne L. Wehrli§, Alex C. Wright*, William T. O'Brien¶, Hidemasa Uematsu*, Felix W. Wehrli*, and Michael E. Selzer‡

Departments of *Radiology and ‡Neurology, University of Pennsylvania Medical Center, 1 Silverstein, 3400 Spruce Street, Philadelphia, PA 19104; §Nuclear Magnetic Resonance Core Facility, Children's Hospital of Philadelphia, Civic Center Boulevard, Philadelphia, PA 19104; and ¶Philadelphia College of Osteopathic Medicine, 4170 City Avenue, Philadelphia, PA 19131

Edited by Marcus E. Raichle, Washington University School of Medicine, St. Louis, MO, and approved October 14, 2002 (received for review April 26, 2002)

Anisotropy of water diffusion in axon tracts, as determined by diffusion-weighted MRI, has been assumed to reflect the restriction of water diffusion across axon membranes. Reduction in this anisotropy has been interpreted as degeneration of axons. These interpretations are based primarily on *a priori* reasoning that has had little empirical validation. We used the experimental advantages of the sea lamprey spinal cord, which contains several very large axons, to determine whether intraaxonal diffusion is isotropic and whether anisotropy is attributable to restriction of water mobility by axon surface membranes. Through the application of magnetic resonance microimaging, we were able to measure the purely intraaxonal diffusion characteristics of the giant reticulospinal axons (20–40 μm in diameter). The intraaxonal apparent diffusion coefficients of water parallel (longitudinal ADC, l-ADC) and perpendicular (transverse ADC, t-ADC) to the long axis were 0.98 ± 0.06 (10^{-3} mm^2/sec) and 0.97 ± 0.11 (10^{-3} mm^2/sec), respectively. In white matter regions that included multiple axons, l-ADCs were almost identical regardless of axon density in the sampled axon tract. By comparison, t-ADCs were reduced and varied inversely with the number of axons (and thus axolemmas) in a fixed cross-sectional area. Thus, diffusion was found to be isotropic when measured entirely within a single axon and anisotropic when measured in regions that included multiple axons. These findings support the hypothesis that the cell membrane is the primary source of diffusion anisotropy in fiber tracts of the central nervous system.

MR microimaging | diffusion-weighted imaging | giant axon | intraaxonal apparent diffusion coefficient | axolemma

Diffusion-weighted MRI (DWI) techniques have been widely applied in the white matter (WM) for detection of damage to axons (1–4) and more recently for determining the orientation of fiber tracks (5, 6) in the brain and spinal cord. These applications invoke diffusional anisotropy, a larger apparent diffusion coefficient (ADC) in longitudinal (l-ADC) orientation than in transverse (t-ADC) orientation, in the WM (7).

Possible causes of the diffusional anisotropy have been subjects of many studies for over a decade (8–10). To date, although these inferences have been derived from simulation and experimental studies, there have been few studies (11, 12) in which the diffusion characteristics of axons have been related directly to axonal anatomy or physiology. This is due largely to limitations in spatial resolution of magnetic resonance (MR) compared with histological methods. In short, it has been possible to obtain MR images of relatively large fields of view, which must be related to the small fields of view achieved with high-power microscopy. Bringing the spatial resolution of MR closer to that of microscopy for diffusion studies will improve correlations of ADCs with histological changes.

The nervous system of the sea lamprey (*Petromyzon marinus*) is unmyelinated. In the spinal cord, the Mauthner and Müller giant reticulospinal axons are of particular interest because of their large caliber (20–40 μm in diameter) (13). Unlike mammals, lampreys exhibit robust spontaneous regeneration of axons after spinal cord injury (14). In numerous histological studies, the anatomy and course of axonal dieback, degeneration, and regeneration after traumatic injury have been well documented (15–18).

We recently developed an MR-microscopy method that could achieve 9×9 μm in-plane resolution in the fixed excised lamprey spinal cord, thus resolving individual Mauthner and Müller axons (19). Applying this MR-microscopic technique to DWI, we report our measurements of regional and intraaxonal ADCs and diffusional anisotropy in the living excised spinal cord of the intact sea lamprey.

Materials and Methods

Animal Protocol. Five intact larval sea lampreys (*P. marinus*, 4–5 years old) were anesthetized in tricaine methanesulfonate (0.1%) for 3–5 min. Excision and handling of the spinal cord have been described in detail (13). Briefly, the spinal cords were excised in ice-cold lamprey Tris-Ringer's buffer (110 mM NaCl/2.1 mM KCl/2.6 mM $CaCl_2$/1.8 mM $MgCl_2$/10 mM Tris buffer, pH 7.4). Each piece of excised cord was immobilized along a thread by a ligation at either end such that the orientation of the longitudinal axis of the axon was perpendicular to the magnetic static field, B_0 (Fig. 1). The cords were placed immediately into a microcapillary (0.9-mm i.d.) and perfused with cold buffer at a rate of 0.4 ml/min. This method of excision of the live cord has been used routinely in electrophysiological studies (20) and has been shown to preserve action potentials in refrigerated pieces of spinal cord for 1 week's experiments after harvest (13). Immediately after MRI, three of the cords were fixed with 2% paraformaldehyde for 12 h. The tissues then were dehydrated in serial ethanol and embedded in paraffin, and tissue blocks were cut 4 mm caudal and rostral to the imaging site. Ten-micrometer transverse paraffin sections were deparaffinized, rehydrated, and blocked in 2% FCS. The primary antibody for lamprey neurofilament (LCM 34, 1:10 in 0.1 M Tris/2% FCS) was applied to the sections and allowed to incubate at 4°C overnight in a humid chamber. The primary antibody was labeled by using the avidin–biotin complex method as described in the ABC kit (Biomedia, Foster city, CA) followed by metal-enhanced diaminobenzidine substrate (Pierce). The sections were counterstained with 0.05% toluidine blue for 10 min and dipped briefly in 0.05% eosin solution. Finally, the sections were dehydrated in serial ethanols, cleared in toluene, and mounted with Permount.

Radio Frequency (RF) Coil Development. The RF probe has been described in detail (19). Briefly, a modified commercial probe

This paper was submitted directly (Track II) to the PNAS office.

Abbreviations: DWI, diffusion-weighted MRI; WM, white matter; ADC, apparent diffusion coefficient; l-ADC, longitudinal ADC; t-ADC, transverse ADC; MR, magnetic resonance; RF, radio frequency.

†To whom correspondence should be addressed at the present address: Department of Radiology, Beth Israel Deaconess Medical Center/Harvard Medical School, 330 Brookline, Boston, MA 02215. E-mail: mtakahas@caregroup.harvard.edu.

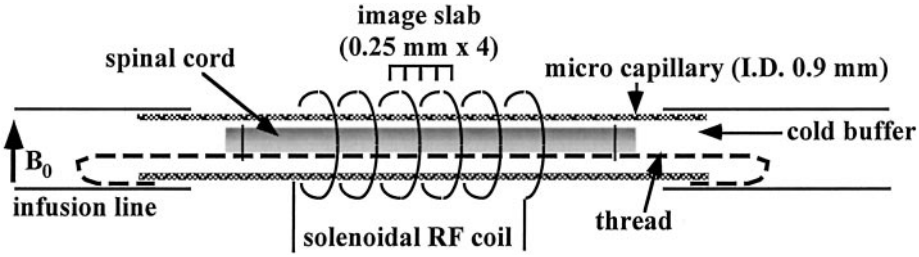

Fig. 1. Scheme of perfusion system for micro diffusion-weighted imaging. Larval sea lampreys (*P. marinus*, 4–5 years old) were anesthetized in tricaine methanesulfonate (0.1%) for 3–5 min. The spinal cords in all animals were excised in Tris-buffered lamprey Ringer's solution. The cords were placed immediately into a capillary micropipet (0.9-mm i.d.) for MRI and perfused with cold buffer. All procedures were performed in an ice bath. The RF probe is a 400-MHz solenoidal transmit/receive RF coil, tuned and impedance-matched via a standard capacitor network that interfaced with the spectrometer's RF transmit/receive chain (coil size: 2.5-mm i.d., 6 mm long, seven turns of 0.5-mm o.d. copper wire).

head consisting of a 400-MHz solenoidal transmit/receive RF coil was tuned and impedance-matched via a standard capacitor network that interfaces with the spectrometer's RF transmit/receive chain (coil size: 2.5-mm i.d., 6 mm long, seven turns of 0.2-mm o.d. copper wire).

Diffusion MRI. Diffusion-weighted micro-MRI was performed on a 9.4 T microimaging system (DMX-400, Bruker Instruments, Karlsruhe, Germany). The system's microimaging accessory consists of three-axis self-shielded magnetic field gradients with 100 G/cm (1,000 mT/m) maximum gradient amplitude in all three channels. Measurements were conducted by using a conventional spin-echo sequence with motion-sensitive gradients perpendicular (transverse, read-encoding) or parallel (longitudinal, slice-encoding) to the long axis of the spinal cord. Four sequential 0.25-mm-thick transverse sections were selected for the diffusion study. Diffusion gradients were applied ($\Delta = 11.3$ msec, $\delta = 6$ msec) with b values of 728.7 and 1,551.2 sec/mm^2 (for t-ADC) and 728.7 and 1,200.0 sec/mm^2 (for l-ADC), respectively (21). Other parameters were: repetition time/echo time = 1,000/21.5 msec, 2.5-mm field of view, 128×128 matrix, 19×19-μm^2 in-plane resolution, eight averages, resulting in a total scan time of $\approx$34 min. Perfusion of the cold buffer was interrupted during imaging to avoid artifacts from flow of the perfusate. Throughout all imaging sessions, the temperature of the specimen was maintained at 6 ± 2°C.

MRI Data Analysis. Signal intensities were measured in the regions of interest, encompassing gray matter and multiple regions of the WM (although there is no myelin in the lamprey, the axon tracts are referred to as WM for convenience) on each image. In the WM, regions of interest were selected carefully within a Mauthner axon and in the dorsal, dorsolateral, and ventral columns (Fig. 2*a*). Signal intensities also were analyzed in the surrounding buffer and across the entire spinal cord. Intensities were measured in air to provide an estimate of noise in each image. ADCs were calculated as the slope of the logarithm of the noise-corrected signal intensities (22) versus the b factors in each region. All ADCs were normalized to the ADC of buffer to correct for temperature variations.

Statistical Analysis. All calculated ADCs were expressed as mean $\pm$ standard deviation. For determination of diffusional anisotropy, a Student's t test was used to test the null hypothesis of isotopic diffusion. Further, differences among the four regions of WM were evaluated with a two-tailed analysis of variance with the Tukey–Kramer multiple-comparison test. Statistical analysis was done by using JMP IN (SAS Institute, Cary, NC).

Results

Microimaging. When fixed spinal cord was imaged by T1-weighted sequences for several hours, it was possible to obtain an in-plane resolution of 9×9 μm (Fig. 2*b*). Under the present conditions, in which imaging was performed by 2D spin-echo sequences and imaging time was limited to 34 min to prevent deterioration of the living cord, in-plane resolution was 19×19 μm, but this was still good enough to resolve several axons including the Mauthner axon (Fig. 3). The Mauthner axons appeared hypointense, and the contrast between them and the surrounding WM was enhanced at higher b values. The ventral column, which includes several giant axons (Müller axons) that are smaller than the Mauthner axon, also appeared darker with respect to the remainder of the cord at the higher b value.

Diffusion Measurement. Table 1 lists the t-ADCs, l-ADCs, and diffusional anisotropy in each region within the live excised spinal cord of the sea lamprey, where the corrected ADCs of the surrounding buffer in both directions were 1.61 ± 0.03 (10^{-3} mm^2/sec) and isotropic. Diffusion within the Mauthner axon was also isotropic as well as that in the gray matter. The other WM regions, and the spinal cord overall, demonstrated diffusional anisotropy. The ADCs varied by WM region (Fig. 4). The t-ADC in the Mauthner axon was the highest, and it was significantly greater ($P < 0.000001$) than the t-ADCs in any other regions. In the other regions, t-ADC values increased in the order: dorsal $\leq$ dorsolateral $<$ ventral. However, l-ADCs of the different WM regions were almost identical ($P > 0.05$). The combination of those values led to increasing diffusional anisotropy in the

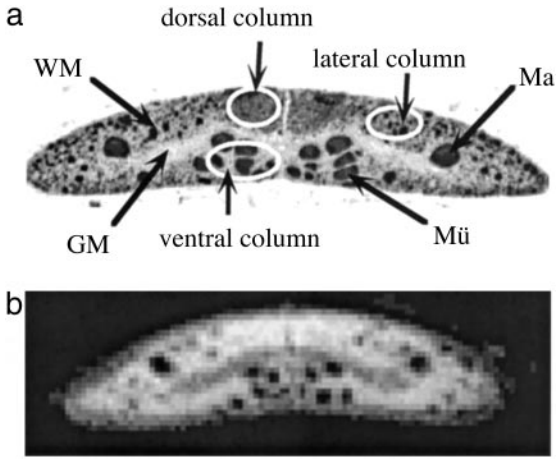

Fig. 2. Histological appearance of the sea lamprey spinal cord. (*a*) The lamprey spinal cord in transverse section immunostained for neurofilaments. Axons stain darkly. White ellipsoids represent a selection of the dorsal, dorsolateral, and ventral columns, respectively. GM, gray matter; Ma, Mauthner axon; Mü, Müller axons. (*b*) For comparison, a T1-weighted micro-MR image of a fixed spinal cord at 9×9-μm resolution.

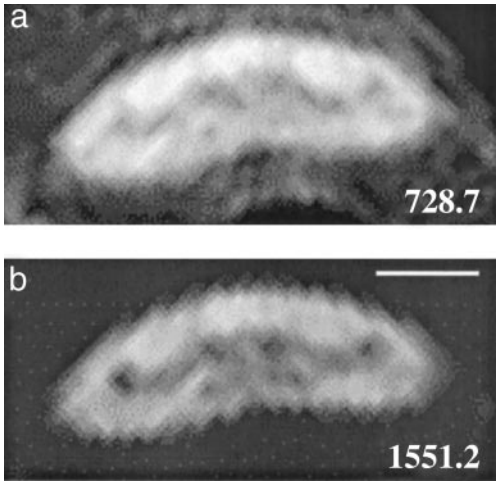

Fig. 3. Transverse diffusion MR images of the living spinal cord. The motion-sensitive gradients are applied perpendicular to the orientation of the axons. Images were obtained with the gradients off (*a*) and on (*b*). Increasing the *b* value from 728.2 to 1,551.2 sec/mm^2 causes rapid loss of signal intensity, particularly in the axon, enhancing the contrast between the Mauthner axon and the surrounding WM tissue. (Scale bar, 100 μm.)

following order: Mauthner axon ≤ ventral < dorsolateral < dorsal column. This order represents increasing density of axons because these areas contain axons of progressively smaller caliber.

After diffusion measurements, it was possible to verify the structural integrity of the spinal cord by fixing the tissue and preparing histological sections. Fig. 5*a* shows a representative diffusion micro-MR image of a piece of living lamprey spinal cord. Fig. 5*b* shows a representative histological microphotograph immunostained for neurofilament from the same piece of spinal cord after it was studied by DWI. Note that the micro-DWI provides structural information almost as detailed as the histologic section. In addition, the histology revealed no post-mortem changes in the cords we examined.

Discussion

We combined a microimaging technique and DWI to determine regional ADCs and diffusional anisotropy in the live excised spinal cord of larval sea lamprey. Although l-ADCs were almost identical, t-ADC showed significant differences among the regions in the WM. Diffusion was found to be isotropic when measured entirely within a single axon and anisotropic when measured in regions that included multiple axons due to the restricted t-ADCs.

At ≈6°C, the intraaxonal diffusion coefficients of water perpendicular and parallel to the long axis of the Mauthner

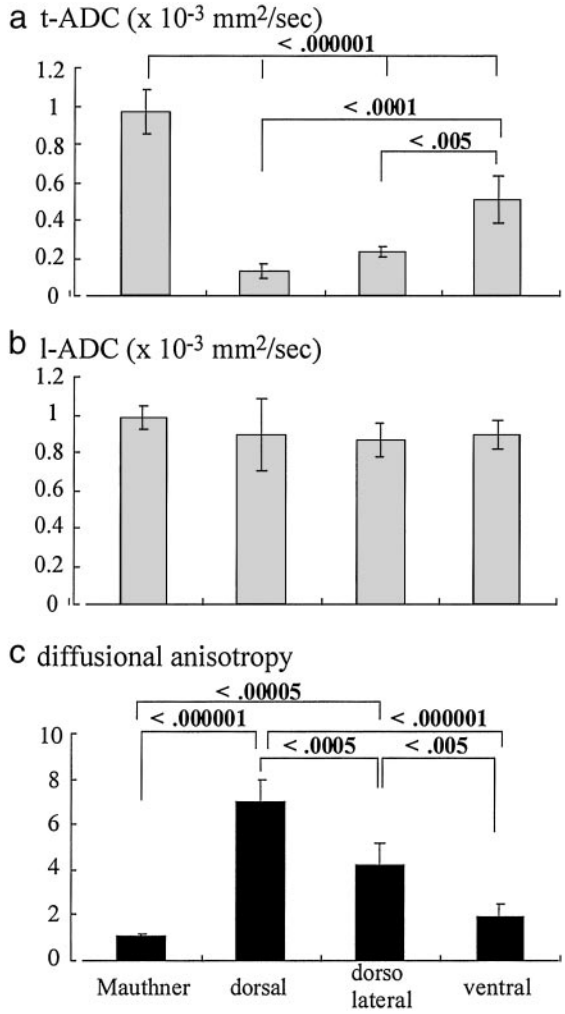

Fig. 4. Anisotropy of water diffusion in axon tracts but not within axons. t-ADC (*a*) and l-ADC (*b*) for water within the Mauthner axon and in different regions of the WM are shown. The degree of anisotropy is shown in *c*. The data represent mean ± standard deviation, which is treated in the multiple-comparison test (Tukey–Kramer).

fibers were 0.97 ± 0.11 (10^{-3} mm^2/sec) and 0.98 ± 0.06 (10^{-3} mm^2/sec), respectively. Thus, pure intraaxonal diffusion was quite rapid and isotropic. The distance of intraaxonal water-molecule movement (diffusion length) in one direction within the current diffusion time, 11 msec, can be calculated as ≈4.6 μm by the equation $d = \sqrt{2Dt}$, where d is diffusion length, D is diffusion coefficient, and t is diffusion time. Thus, regarding

Table 1. t-ADC, l-ADC, and diffusional anisotropy in the live excised spinal cord of the larval sea lamprey (n = 5)

Regions	t-ADC, 10^{-3} mm^2/sec	l-ADC, 10^{-3} mm^2/sec	l-ADC/t-ADC	Diffusion
Entire spinal cord	0.32 ± 0.06	0.80 ± 0.08	2.67 ± 0.71	Anisotropic
Gray matter	0.30 ± 0.03	0.28 ± 0.04	0.97 ± 0.24	Isotropic
WM				
Mauthner axon	0.97 ± 0.11	0.98 ± 0.06	1.04 ± 0.12	Isotropic
Dorsal	0.14 ± 0.03	0.89 ± 0.19	7.03 ± 0.95	Anisotropic
Dorsolateral	0.23 ± 0.04	0.87 ± 0.09	4.17 ± 1.03	Anisotropic
Ventral	0.50 ± 0.14	0.89 ± 0.09	1.91 ± 0.62	Anisotropic

Values are expressed as mean ± standard deviation. The anisotropic diffusion was determined by the statistical significance ($P < 0.05$) in the Student's t test between the t-ADC and the l-ADC.

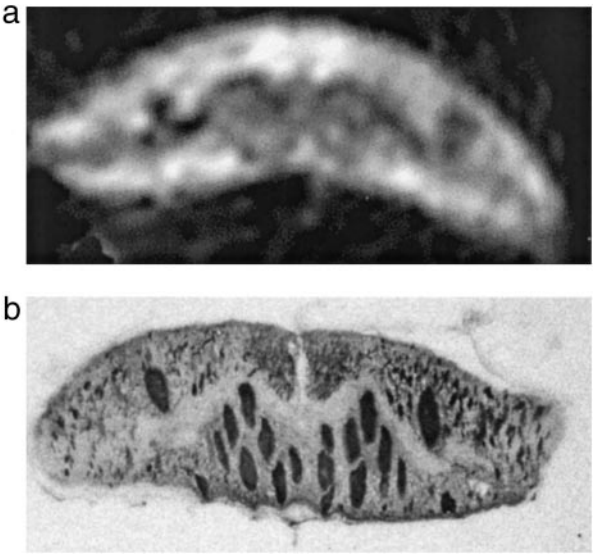

Fig. 5. Preservation of histological structure of the spinal cord after MR microimaging. (*a*) A diffusion-weighted MR microimage ($19 \times 19 \times 250$ μm^3) with the motion-sensitive gradients on read direction (b = 1,551 sec/mm^2). (*b*) A neurofilament-immunostained transverse histological section from the same piece of spinal cord after imaging. Note that the micro-DWI provides structural information almost as detailed as a histological section. Aside from slight deformity of the cord due to confinement in the micropipet, the histological appearance showed no postmortem changes.

the probability of the existence, most axoplasmic water molecules in the giant axon ($\approx$40 μm in diameter) would not hit the boundary during the measurement so that the measured intraaxonal t-ADC should represent free diffusion. On the other hand, the measurement can reflect restricted diffusion in all other WM regions, because the mean diameters of the axons or mean spacing of extracellular spaces are <5 μm, and thus some boundaries would be included (13, 23).

Possible causes of the MR-derived diffusion anisotropy observed in axonal tracts of WM have been postulated to be the cell membrane, multiple layers of myelin sheath (21, 24), axonal transport, and/or the microstructures within axons such as microtubules, myosin, or neurofilaments (25). To date, there have been few studies demonstrating diffusion coefficients within a single axon, and thus it is unknown whether intraaxonal diffusion is restricted perpendicular to the long axis. Beaulieu and Allen (26, 27) reported that the several unmyelinated nerves in a garfish showed reduced diffusional anisotropy after depolymerization of intraaxonal microstructures, indicating that intraaxonal microstructures and axonal transport were not the sole determinants of diffusional anisotropy. Another study by this group of the freshly excised giant axon of the squid showed slightly anisotropic intraaxonal diffusion (28). Our present results, demonstrating consistently isotropic intraaxonal diffusion, eliminate intraaxonal factors as sources of anisotropic diffusion in WM. Moreover, because the lamprey nervous system lacks myelin, the presence of anisotropic diffusion in the WM of this animal shows that myelin is not necessary for diffusional anisotropy. Similar conclusions were arrived at by less direct means in studies of mammalian central nervous system (1, 27). The anisotropic diffusion that contained multiple axons resulted from reduced t-ADCs, whereas l-ADCs were similar to those of the Mauthner axon. These results are the best explained as sole determinant of restriction by the cell membrane.

A number of recent studies have demonstrated a biexponential diffusion behavior in tissues. Initial interpretations attributed these slow and fast diffusion components to ADCs in intra- and extracellular spaces (ICSs and ECSs), respectively (29). However, the estimated fractions based on biexponential diffusion measurements are inconsistent with the known ICS and ECS volume fractions in tissue based on this assumption. In the present study, time constraints prevented us from acquiring data that would permit estimation of biexponential ADCs. However, our measured monoexponential ADCs, which were calculated with b values ranging from 700 to 1,500 sec/mm^2, must be intermediate between the fast and slow components if we would have measured them. The intraaxonal ADC in the small fibers can be assumed to be the same as that in the Mauthner axon because the contents/structures of the axons are similar (23). Nevertheless, the values of t-ADC (10^{-3} mm^2/sec) in the subregional WM that includes multiple axons were much lower, 0.14–0.50, than the pure intraaxonal ADC, $\approx$0.98. This result implies that the slow component of multiexponential ADCs is not simply the intracellular ADC, although the slow component is likely influenced by the intracellular diffusion coefficient. Therefore, we conclude that the MR-derived multiple-exponential ADC, measured conditions that manifest diffusion restriction, reflects the ADCs of the ICS, the ECS, membrane spacing, and membrane permeability when the "diffusion time" is long enough, which is consistent with our previous work (30).

The anatomy of the WM in the lamprey spinal cord has been studied in detail (13, 23). Features of WM anatomy relevant to our purposes include: (*i*) the diameters of the axons range from 0.5 to 50 μm, (*ii*) densely packed axons, many of which are too small to resolve by light microscopy, are found in the dorsal columns, and (*iii*) many medium-sized axons are present in the dorsolateral and lateral columns, and still larger axons (the Müller reticulospinal axons) are found in the ventral columns. Thus the mean diameter of axons increases, and the axons are progressively less densely packed, in the following order: dorsal, dorsolateral, and ventral columns. The t-ADCs we measured also increased in the same order. The results may imply that these measurements of t-ADC are sensitive to the diameter of axons and to fiber packing density and are in a good semiquantitative agreement with those of simulations (9, 10).

It has been documented that sea lamprey axons regenerate after spinal transection. Early after transection, axons die back from the transection site. Thereafter, axons regenerate from the proximal stump across the injury site (15). During regeneration, many fibers produce several small sprouts, some of which are subsequently pruned (14). The remaining axons then enlarge but often never regain their original diameter (31). Our results demonstrate that ADC measurements are sensitive to the presence, number, and diameter of axons in the normal cord, which implies that determination of ADC (t-ADC, l-ADC, and the diffusional anisotropy) can provide a method for monitoring the anatomic changes that accompany degeneration and regeneration of axons after injury in sea lampreys if images are acquired with adequate spatial resolution. In clinical studies, where it may not be possible to obtain sufficient spatial resolution to identify individual fiber tracks, the results might be determined as weighted averages of regional changes. Although this might reduce the precision of measurements of axonal changes, it would remain the most sensitive means available for monitoring the structural responses to injury. Although it seems that myelin is not the prime determinant of diffusional anisotropy, it remains possible that, in the myelinated WM of mammals, the extent of myelin loss and recovery may influence the ADCs observed.

This research was supported by National Institutes of Health Grants R01 NS4180, R01 NS25921, R01 NS14837, and R01 NS25581.

1. Ono, J., Harada, K., Takahashi, M., Maeda, M., Ikenaka, K., Sakurai, K., Sakai, N., Kagawa, T., Fritz-Zieroth, B. & Nagai, T. (1995) *Brain Res.* **671,** 141–148.
2. Ono, J., Harada, K., Mano, T., Sakurai, K. & Okada, S. (1997) *Pediatr. Neurol.* **16,** 63–66.
3. Ford, J. C., Hackney, D. B., Alsop, D. C., Jara, H., Joseph, P. M., Hand, C. M. & Black, P. (1994) *Magn. Reson. Med.* **31,** 488–494.
4. Clark, C. A., Werring, D. J. & Miller, D. H. (2000) *Magn. Reson. Med.* **43,** 133–138.
5. Mori, S., Crain, B. J., Chacko, V. P. & van Zijl, P. C. (1999) *Ann. Neurol.* **45,** 265–269.
6. Makris, N., Worth, A. J., Sorensen, A. G., Papadimitriou, G. M., Wu, O., Reese, T. G., Wedeen, V. J., Davis, T. L., Stakes, J. W., Caviness, V. S., *et al.* (1997) *Ann. Neurol.* **42,** 951–962.
7. Moseley, M. E., Kucharczyk, J., Asgari, H. S. & Norman, D. (1991) *Magn. Reson. Med.* **19,** 321–326.
8. Szafer, A., Zhong, J. & Gore, J. C. (1995) *Magn. Reson. Med.* **33,** 697–712.
9. Ford, J. C. & Hackney, D. B. (1997) *Magn. Reson. Med.* **37,** 387–394.
10. Ford, J. C., Hackney, D. B., Lavi, E., Phillips, M. & Patel, U. (1998) *J. Magn. Reson. Imaging* **8,** 775–782.
11. Hsu, E. W. (1997) *Magn. Reson. Med.* **37,** 624–627.
12. Grant, S. C. (2001) *Magn. Reson. Med.* **46,** 1107–1112.
13. Selzer, M. E. (1979) *Brain Res.* **163,** 181–193.
14. Lurie, D. I. & Selzer, M. E. (1991) *J. Comp. Neurol.* **306,** 409–416.
15. Selzer, M. E. (1978) *J. Physiol. (London)* **277,** 395–408.
16. Yin, H. S. & Selzer, M. E. (1983) *J. Neurosci.* **3,** 1135–1144.
17. Davis, G. R., Troxel, M. T., Kohler, V. J., Grossmann, E. M. & McClellan, A. D. (1993) *Exp. Brain Res.* **97,** 83–95.
18. Zhang, G. & Selzer, M. E. (2001) *Exp. Neurol.* **167,** 304–311.
19. Wright, A. C., Wehrli, S. L., Zhang, G., Takahashi, M., Hackney, D. B., Selzer, M. E. & Wehrli, F. W. (2002) *J. Neurosci. Methods* **114,** 9–15.
20. Mackler, S. A. & Selzer, M. E. (1987) *J. Physiol. (London)* **388,** 183–198.
21. Moseley, M. E., Cohen, Y., Kucharczyk, J., Mintorovitch, J., Asgari, H. S., Wendland, M. F., Tsuruda, J. & Norman, D. (1990) *Radiology (Easton, Pa.)* **176,** 439–445.
22. Miller, A. J. & Joseph, P. M. (1993) *Magn. Reson. Imaging* **11,** 1051–1056.
23. Pijak, D. S., Hall, G. F., Tenicki, P. J., Boulos, A. S., Lurie, D. I. & Selzer, M. E. (1996) *J. Comp. Neurol.* **368,** 569–581.
24. Takahashi, M., Ono, J., Harada, K., Maeda, M. & Hackney, D. B. (2000) *Radiology (Easton, Pa.)* **216,** 881–885.
25. Le Bihan, D., Turner, R., Douek, P. & Patronas, N. (1992) *Am. J. Roentgenol.* **159,** 591–599.
26. Beaulieu, C. & Allen, P. S. (1996) *Magn. Reson. Med.* **36,** 39–44.
27. Beaulieu, C. & Allen, P. S. (1994) *Magn. Reson. Med.* **31,** 394–400.
28. Beaulieu, C. & Allen, P. S. (1994) *Magn. Reson. Med.* **32,** 579–583.
29. Niendorf, T., Dijkhuizen, R. M., Norris, D. G., van Lookeren Campagne, M. & Nicolay, K. (1996) *Magn. Reson. Med.* **36,** 847–857.
30. Chin, C. L., Wehrli, F. W., Hwang, S. N., Takahashi, M. & Hackney, D. B. (2002) *Magn. Reson. Med.* **47,** 455–460.
31. Swain, G. P., Snedeker, J. A., Ayers, J. & Selzer, M. E. (1993) *J. Comp. Neurol.* **336,** 194–210.